

## Article

# Study of Crack Generation and Expansion Behavior of Frame-Supported Float Glass after Heat Exposure

Yanni Zhang <sup>1,2,\*</sup>, Luoxin Huang <sup>1</sup>, Jun Deng <sup>1,2</sup>, Zhichao Feng <sup>1</sup>, Dan Yang <sup>1</sup>, Xuemeng Liu <sup>1</sup> and Shuai Zhang <sup>1</sup>

<sup>1</sup> School of Safety Science and Engineering, Xi'an University of Science and Technology, 58 Yanta Middle Road, Xi'an 710054, China; huangluoxin\_ad@163.com (L.H.); dengj518@xust.edu.cn (J.D.); m17791213850@163.com (Z.F.); yangdan\_ad@163.com (D.Y.); xust18161798525@163.com (X.L.); 15929525995@163.com (S.Z.)

<sup>2</sup> Xi'an Key Laboratory of Urban Safety and Fire Rescue, 58 Yanta Middle Road, Xi'an 710054, China

\* Correspondence: zyn2099@xust.edu.cn

**Abstract:** Float glass installed with frame supports is broadly exploited in building construction. In a fire environment, the breakage of float glass significantly influences the dynamic development of the fire within the building space. The thermal rupture behavior of the frame-supported float glass subjected to thermal loading is carefully examined using a self-built experimental system. The designed system is aimed at capturing crucial behavioral parameters. The experimental study reveals that the main reason for the breakage of the frame-supported float glass is the temperature difference on the glass surface, with a critical temperature difference of approximately 65 °C. The crack starts at the edge of the glass surface where the temperature difference is maximum and then rapidly expands. By intersecting the cracks, a crack island is configured, which is not dislodged under the stress of the supporting frame and the surrounding glass. A thermomechanical and micro-geometric model of the frame-supported float glass is developed based on the PFC<sup>2D</sup> program to show further the micro-crack expansion pattern of the frame-supported float glass under thermal loading. This scrutiny provides theoretical guidance for installing and using frame-supported float glass in construction projects and identifying fire evidence.

**Keywords:** frame support; float glass; thermal load; thermal fracture law; thermodynamic model; microcrack extension



**Citation:** Zhang, Y.; Huang, L.; Deng, J.; Feng, Z.; Yang, D.; Liu, X.; Zhang, S. Study of Crack Generation and Expansion Behavior of Frame-Supported Float Glass after Heat Exposure. *Fire* **2023**, *6*, 281. <https://doi.org/10.3390/fire6070281>

Academic Editor: Ali Cemal Benim

Received: 25 May 2023

Revised: 16 July 2023

Accepted: 17 July 2023

Published: 22 July 2023



**Copyright:** © 2023 by the authors. Licensee MDPI, Basel, Switzerland. This article is an open access article distributed under the terms and conditions of the Creative Commons Attribution (CC BY) license (<https://creativecommons.org/licenses/by/4.0/>).

## 1. Introduction

As one of the most crucial components commonly exploited in urban high-rise buildings, float glass is extensively utilized in doors, windows, ceilings, walls, and other parts of buildings [1]. As a brittle material with relatively weak mechanical properties, float glass is susceptible to breakage and dislodgement under the action of fire heat loads, which in turn can give rise to new fire spread channels, accelerating the spread of fire and threatening the safety of the building structure and occupants. The frame-supported installation approach is the most common way of installing glass in construction projects [2,3]. Analyzing the dynamic performance of frame-supported float glass under thermal loads and studying the physical and chemical properties of the glass can help reveal the fracture mechanism of frame-supported float glass and further elucidate the relationship between glass breakage time and temperature difference between the sheltered and non-sheltered areas of glass in building fires and explore the relationship between glass cracking and the degree of damage and collapse behavior [4–6]. Therefore, understanding the safety properties of glass components in construction engineering is crucial for building fire safety and fire accident investigation.

Emmons [7] first suggested in 1986 that the breakage of glass in a fire is significant research value. Since then, scholars have scrutinized the mechanism of glass breakage

through many experiments and numerical simulations. Skelly et al. [6] designed a simulation compartment to study the breaking process of glass in an actual building fire. Finally, they found the theoretical, critical temperature difference that leads to the breaking of edge-protected glass. Pagni et al. [8,9] developed the glass breakage program BREAK1 accounting for the coupling between the heat transfer model and the glass breakage criterion. Their established numerical model could predict the first occurrence of glass breakage and calculate the temperature field on the glass surface. Harada et al. [10] predicted the first rupture time of glass based on box-fired heating conditions and showed it through a simple formula. Based on many studies and experiments, Pope et al. [11] proposed a Gaussian glass fracture model and applied this model to fire dynamics simulation software. Hietaniemi J [12] analyzed the probability of glass shedding and breakage in a fire environment utilizing Monte Carlo simulation and BREAK1. Ni et al. [13] investigated the fire performance of double facades made with double glazing in three different heat release rate fire scenarios. Wang et al. [14–18] utilized a finite element program to assess the glass crack expansion process in the context of differences in boundary constraint methods and thermal impacts by employing a large amount of fundamental theory. Wong et al. [19] studied the fallout behavior of glass samples under thermal radiation and established a probabilistic prediction model of glass fallout. Debuysier et al. [20] further studied the thermal characteristics and mechanical behavior of laminated glass in fire and proposed a numerical heat transfer model based on the experiment. Under different working conditions, Wang et al. [21–24] investigated the fracture mechanism of glass curtain walls under a fire environment through full-scale experiments and numerical simulation. They obtained the fracture rule of glass curtain walls under different installation methods in a fire environment. In addition to the crack observation and experiment of glass, Mauro et al. [4] also studied the molten state of glass at high temperatures, proposed the visco-temperature relationship model of glass, and profoundly discussed the glass transition, which is also helpful in describing the cracking mechanism of glass.

In 2017, Chiara [25] carried out a systematic review of the research on glass structures in fire, comprehensively introduced the research results produced in this field in recent decades, thoroughly discussed the existing design methods and existing problems, and pointed out that the future research should pay attention to the adoption of multidisciplinary methods. Since then, scholars have conducted additional detailed and in-depth studies in this field. Lu et al. [26] performed thermal load tests on five different types of point-supported glass curtain walls, established thermodynamic models, and performed optimization simulations using the constrained optimization of the quadratic approximation method to obtain better thermal resistance performance of the glass facades. Chen et al. [27,28] examined the simulation and design of various fire scenarios based on the developed programs to solve for the glass temperature field and quasi-dynamic crack expansion. The first breakage time and quasi-static dynamic crack expansion process of glass under different conditions were then predicted. Wang et al. [29,30] conducted an in-depth exploration of the relevant studies from the two perspectives of experiment and simulation to provide further a theoretical basis for the fire prevention of building glass curtain walls. Firstly, three different importance analysis methods are used to find that the type of glass, fire location and installation method are crucial factors for the fire protection of building glass curtain walls. Second, by validating the finite element method model, it was found that the difference in the stress distribution due to size and shape effects is the main reason for the different fire resistance of glass surfaces. In terms of the thermal behavior of glass melting, Cassetta et al. [5] further studied the correlation between vibrational-elastic properties and viscosity. A vibrational property of parental glasses is proposed, and the glass behavior can be predicted based on elasticity. In addition, some scholars have studied the thermal performance of lightweight concrete walls containing glass from the architectural perspective and deduced the influence of different glass ratios on the fire resistance of walls, which can also provide some referential conclusions for the thermal fracture behavior of glass [31,32].

In general, there has been a great deal of research on glass installation methods, glass materials, temperature domains, and crack solution calculations by domestic and international scholars. However, there are still extremely few concrete studies on the properties of frame-supported glasses in terms of thermal breakdown behavior, and it is difficult to monitor the true dynamical process from microscopic damage accumulation to macroscopic damage of glasses due to the existing testing conditions and testing costs. This paper aims to provide a theoretical reference for scientific installation and fire investigation of framed glass in buildings by studying thermal fracture theory and the microscopic damage process of framed glass under elevated temperature loading conditions.

The glass was therefore chosen as the object of study, and full-scale experiments and numerical simulations of fire were performed on frame-supported glass using a self-built experimental bench and particle flow software. We have analyzed the characteristic behavior parameters, such as surface temperature, crack initiation location, and expansion pattern, to determine the macroscopic thermal breakup behavior of frame-supported float glass. In addition, the microfracture process of glass under thermal load has been simulated with the PFC<sup>2D</sup> code to reveal the mechanism of microcrack expansion under thermal load and thus to understand the fracture behavior and mechanism of frame-supported glass.

## 2. Experimental Setup and Methods

### 2.1. Experimental Description

The glass curtain wall engineering standard is utilized to design a glass fire experiment platform capable of meeting the experimental requirements. The glass used in this experiment is float glass, which is widely used in frame-supported glass curtain systems due to its excellent performance and stable physical and chemical properties. Therefore, float glass is selected as the research object in this paper to enhance the practical engineering significance. The float glass used in this experiment is produced by China Pingxiang Float Glass Factory. Table 1 shows the correspondence between the surface viscosity and the bulk viscosity of the glass, Table 2 shows the chemical composition of the glass, and the proportion of each chemical composition is presented as a percentage by weight. In addition, its visible light transmission ratio is 84 percent. As shown in Figure 1, in the fire simulations system, an oil pan of dimensions 500 mm × 500 mm is exploited as the fuel container, and a mass loss balance is arranged below the oil basin. The glass support frame consists of four stainless steel edges capable of withstanding high temperatures, with the edges shading the float glass to a width of 20 mm, and the glass support frame is placed 350 mm from the center of the fire source. To make the physical parameters of the float glass the same in the experiment, all float glass is cut in one piece, with a size of 1000 mm × 1000 mm × 6 mm, and the edges are ground.

**Table 1.** The corresponding relation between surface viscosity and bulk viscosity of float glass.

Pair Value of Viscosity	Noumenon (Temperature for the Corresponding Viscosity)	Tin Level (Temperature for the Corresponding Viscosity)
lg15	420	447
lg14	509	524

**Table 2.** Chemical composition of float glass.

Oxide	SiO <sub>2</sub>	Na <sub>2</sub> O + K <sub>2</sub> O	CaO	MgO	Al <sub>2</sub> O <sub>3</sub>	Fe <sub>2</sub> O <sub>3</sub>
Wt%	72	13.9	8.5	3.9	1.4	0.1

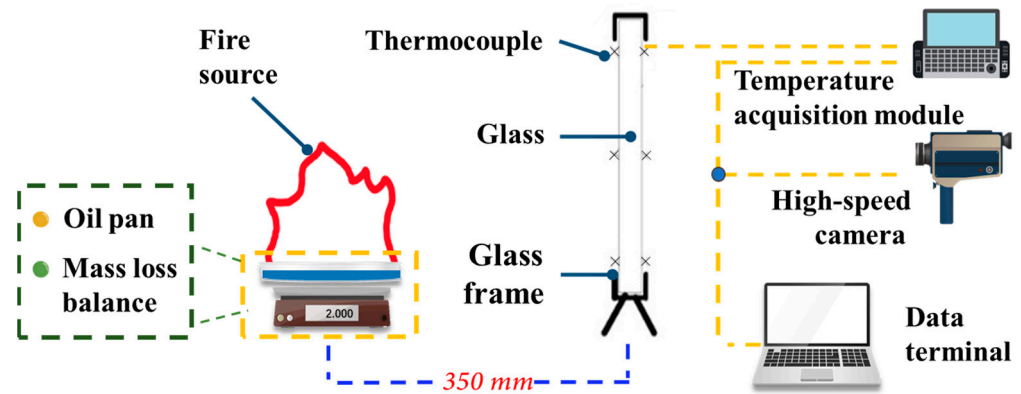


Figure 1. The platform of the glass fire experiment.

A Memrecam HX-1E high-speed camera is selected to record the characteristic glass breakage parameters. The glass surface temperature is measured by a K-type patch thermocouple from 0 °C to 800 °C. Further, the air temperature is measured by a NiCr-NiSi armored thermocouple J fixed at 5 mm from the center of the float glass towards the fire face from 0 °C to 1300 °C. The distribution of thermocouples on the glass surface has been presented in Figure 2, where the lowercase letters denote thermocouples at the float glass to fire surface position, while the uppercase letters represent thermocouples at the float glass backfire surface. To effectively avoid experimental errors, four sets of repetitive experiments are conducted, and the final experimental results are averaged.

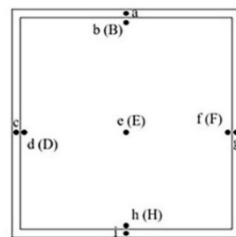


Figure 2. The thermocouple distribution on the float glass surface.

## 2.2. Numerical Simulations

### 2.2.1. Thermodynamic Equations in Discrete Bodies

The PFC<sup>2D</sup> program usually uses a microstructure model containing a thermal memory and a heat pipe to predict the temperature field. Figure 3 shows a schematic representation of the heat transfer within the activated heat pipes between the thermal storages. There exists a coincident contact between the heat pipes and the particles, and the heat pipes are activated when there is an overlapping area or a connection bond between the two particles. During loading, the number of activated heat pipes changes, and the thermal conductivity of the material varies if new connection bonds are created or broken in the microscopic model of the material.

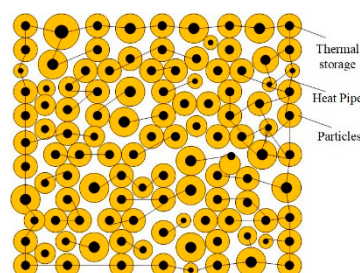


Figure 3. The relationship between particles, heat source, and heat pipes in the PFC<sup>2D</sup>.

The transformation of the heat transfer equation for a continuum to the heat transfer equation for a discrete body is obtainable:

$$-\sum_{p=1}^N Q^{(p)} + Q_v = mC_v \frac{\partial T}{\partial t} \tag{1}$$

where  $Q_v = V \cdot q_v$  denotes the heat source intensity of the discrete,  $m$  represents the mass of the discrete, and  $C_v$  is the specific heat capacity.

In discrete element modeling of the problem, the thermal expansion of the particles and the connecting bonds between them describes the thermal strain of the material. The change in the thermal strain can be achieved by changing the radius of the particles. This issue can be formulated by:

$$\Delta R = \alpha R \Delta T \tag{2}$$

in which  $\alpha$  denotes the linear coefficient of the thermal expansion,  $\Delta T$  represents a known temperature difference, and  $\Delta R$  is the variation of the particle radius.

If a bond exists between each pair of particles and the heat pipes would be active, then a change in the temperature will cause a change in the bond length and the force exerted on the bond. The change in  $L$  due to a change in the temperature only affects the change in the normal force as follows:

$$\Delta F^n = -k^n A \Delta U^n = -k^n A (\alpha \cdot L \cdot \Delta T) \tag{3}$$

where  $k^n$  and  $A$  to represent the normal stiffness and cross-sectional area of the bond,  $\alpha$  is the linear coefficient of thermal expansion pertinent to the bond, and  $\Delta U$  denotes the amount of overlap between the two contacting particles.

### 2.2.2. The Discrete Element Modeling of the Float Glass

The main idea of the particle discrete element model is to divide the computational model into several independent particle bodies and iterate the calculation according to the force relationship between the particles using Newton’s second law of motion and the force-displacement law until the predetermined conditions are satisfied and then the calculation is stopped. The motion of a circular particle medium and its interactions through the discrete unit method is simulated, and the macroscopic motion laws of the whole system are appropriately extracted. Figure 4 shows a simplified discrete element model of the float glass with 24,157 particles, a glass size of 1000 × 1000 mm, a four-sided frame constraint, and a heated surface, and a transient analysis using a coupled temperature-stress sequence method with a set temperature and stress iteration step of  $1 \times 10^{-3}$  s.

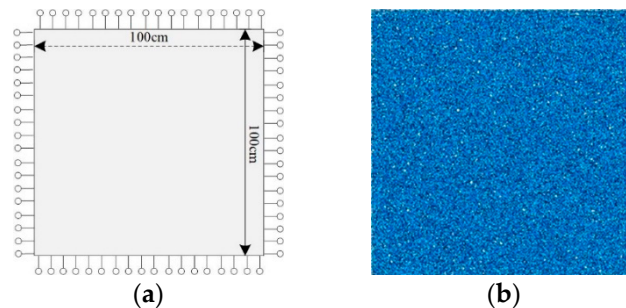


**Figure 4.** The discrete element model of the float glass. (a) Physical model; (b) Discrete element model.

The PFC<sup>2D</sup> program establishes a two-dimensional parallel bonding model with closely spaced and randomly distributed particles. The grains are described by adjusting the particle size and setting the model porosity to match the material porosity to achieve microscopic similarity between the discrete element model and the real structure. The microscopic parameters, such as parallel bonding stiffness ratios and normal and tangential

bond strengths, are essentially determined by “trial and error” adjustment, and the control parameters have been presented in Table 3.

**Table 3.** The control parameters for numerical examples of thermodynamically coupled granular flow in the float glass.

Name of Parameter	Description of Parameters	Value
	$\rho$ Particle specific gravity/(kg/m <sup>3</sup> )	2254
	$\mu$ Inter-particle friction coefficient	0.5
	$\lambda$ Radius magnification factor	1.0
	$E_c$ Inter-particle contact modulus	30
	$E_c$ Parallel bond modulus	30
Fine view control parameters of the PFC model	$k_n/k_s$ Particle stiffness ratio	2.0
	$k_n/k_s$ Parallel bond stiffness ratio	2.0
	$\sigma_c$ (mean) Parallel bond normal strength average	220
	$\sigma_c$ (std.dev) Parallel bond normal strength standard error	55
	$\tau_c$ (mean) Parallel bond tangential strength average	220
	$\tau_c$ (std.dev) Parallel bonding tangential strength standard error	55
	$C_v$ Specific heat/(J/(kg·°C))	1400
	$\eta$ Thermal resistance/(°C/Wm)	0.86

The temperature load after a building fire mainly considers fixed fire load, moving fire load, heat release rate, and fire duration. In the present paper, the ISO834 standard fire model is utilized to simulate high-temperature load, per the following relation:

$$T = 20 + 345\log_{10}(8t + 1) \quad (4)$$

### 3. Results and Discussion

#### 3.1. The Temperature Fields of the Glass Surface and Air

Based on the research of Wang Yu and other investigators [27,28], it can be seen that the maximum temperature gradient on the glass surface is mainly concentrated between the exposed surface of the glass and the sheltered surface of the frame. Therefore, the present experiment is carried out by placing thermocouples on the surface of the float glass. These are positioned about 5 mm from the center of the fireward surface of the float glass to monitor the temperature change of the glass surface and air. The experimentally obtained results have been demonstrated in Figure 5.

The overall increase in the temperature of the frame-supported float glass under high-temperature thermal loads is observable. As the non-shaded area of the float glass is directly exposed to the thermal radiation in the air, the temperature rises in the non-shaded area measured by the thermocouples e, f, b, d, and h is relatively fast and follows the same trend, indicating a uniform distribution of the heat load on the surface of the non-shaded area of the float glass. While the temperature rises in the shaded area measured by thermocouples a, g, c, and i are relatively slow because the four sides of the float glass are subjected to the shading effect of the metal frame. The temperature rise is relatively low compared to the glass in the non-shaded area, where the measurement point a is located in the shaded area; nevertheless, the hot smoke from the fire source rises under the action of the plume, resulting in the measurement point being in the hot air layer and the temperature rise is faster compared to the other shaded areas. The difference in the rate of temperature rise between the shaded and unshaded areas of the glass surface leads to a temperature gradient on the glass surface.

Furthermore, since glass is a poor conductor of heat, it takes more time for heat to transfer from the glass to the backside of the fire. The temperatures measured by the thermocouples b, d, h, and e on the glass to the fireside are higher than those measured by thermocouples B, D, H, and E on the backside of the fire. It implies a remarkable temperature gradient in the glass thickness direction.

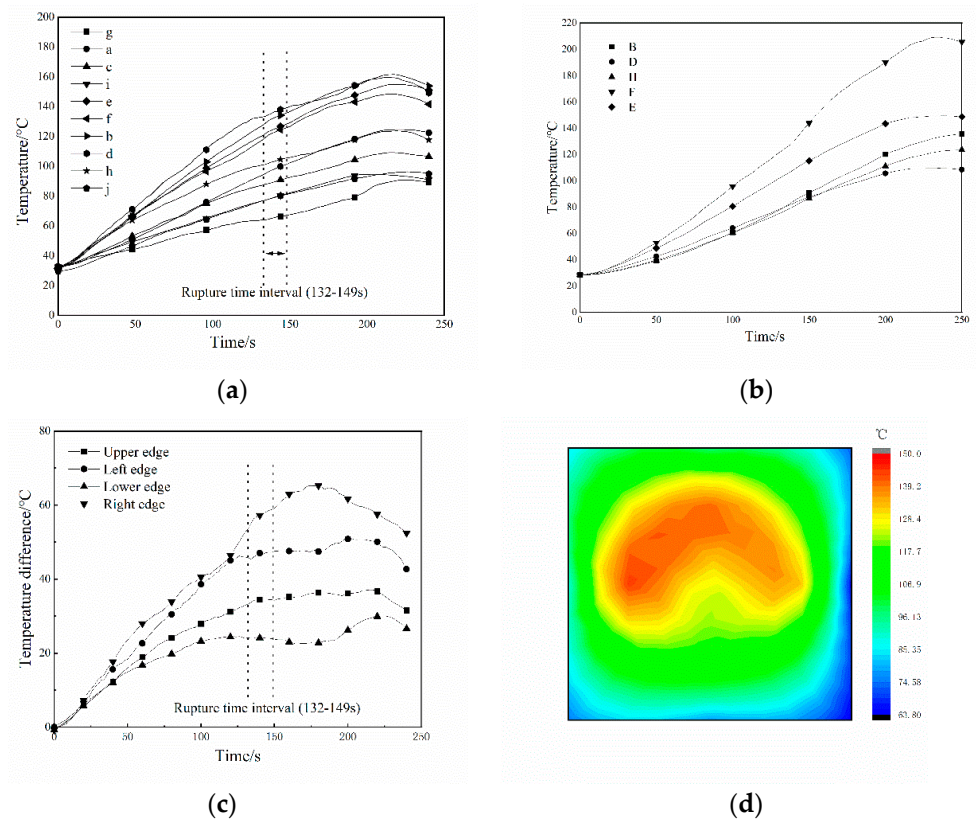


**Figure 5.** Temperature distribution at the first break of the frame-supported float glass. (a) Average thermocouple temperature change on the fireward side of the glass (Left). (b) Average thermocouple temperature change on the backward side of the glass (Right) (c) Plots of the average temperature difference at each edge of the glass surface as a function of time (Left). (d) Variation in the surface and air temperatures of the float glass (Right).

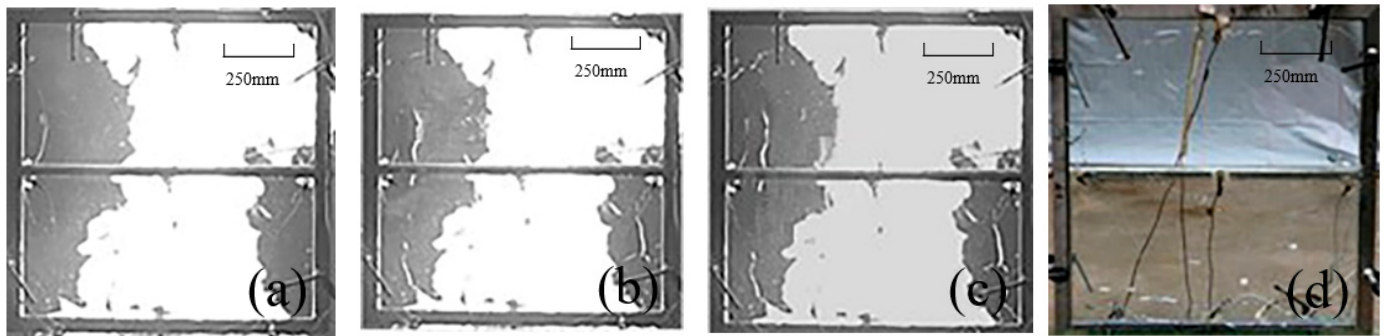
If the temperature gradient increases and the resulting thermal stress is higher than the local load on the glass surface, the glass will break. The temperatures of the shaded and unshaded areas at the moment of glass breakage in each group of experiments are compared. Then the maximum temperature difference of the glass is evaluated. It is detectable that the experimental critical temperature difference for the breakage of the frame-supported float glass is about 65 °C. These results indicate that the temperature difference between the shaded and unshaded areas of the frame-supported float glass is the main cause of the rupture phenomenon under thermal loading.

### 3.2. Time to First Breakage and Crack Evolution of the Glass

The glass’s first breakage time is from the start of ignition to when the glass first cracks. As a substantial characteristic parameter of the thermal breakage behavior of the glass, the time of the first breakage has a crucial influence on the dynamic development of building fires. The first break time of the float glass in the test is determined from the image recordings of the high-speed camera. The breakage of the float glass occurs in all four groups of experiments. The temperature corresponding to the first break of the float glass is shown in Figure 5. And the first break time of the float glass and the location of the crack initiation have been presented in Table 4. The crack expansion and the final form of the frame-supported float glass are demonstrated in Figure 6, and the glass in the picture is a full-size shot.

**Table 4.** Time of the first breakage and location of the crack initiation in the float glass.

Experiment Number	Time of First Breakage of Glass (s)	Maximum Temperature Difference Masking Edge	First Crack Location
1	132	Left edge (d)	Left edge (d)
2	145	Right edge (f)	Right edge (f)
3	136	Right edge (f)	Right edge (f)
4	149	Right edge (f)	Right edge (f)

**Figure 6.** The crack extension and final shape of the frame-supported float glass, (a) Initial crack initiation, (b) Crack initiation location, (c) Crack extension direction and (d) Final crack pattern.

The average time to the first cracking of the frame-supported float glass in the experiment is 140 s. The high-speed camera recording shows that the cracks sprout from the left and right edges of the glass due to the large temperature difference at the glass level; therefore, the cracks appear more frequently from the left and right sides of the glass. By comparing the location of the crack initiation and the area of maximum temperature difference, it is found that the cracks all initiate from the edge of the glass surface where the temperature difference is the greatest. The cracks appear from the edge and then rapidly expand to the central area of the glass or other edges before stopping to expand. Eventually, two to three bifurcated cracks are observed on each main crack, with crack islands forming after the cracks intersect. Due to the constraint of the glass support frame and the stress effect of the surrounding glass, the crack islands remain in their original positions (i.e., no cracked island is dislodged in any of the four sets of experiments).

### 3.3. The Morphology of the Microcrack Rupture

Using the PFC<sup>2D</sup> combined with Fish language to prepare the loading command flow and adjust the measurement sphere function, the microcracking characteristics of the calculated model during high-temperature loading are obtained through iterative calculation, as shown in Figure 7, where the red areas exhibit the rupture regions. When loading steps are less than 5270, microcracks are produced on the glass surface, and the rupture range is small. As the temperature rises, the thermal stress on the glass surface gradually increases, the number of microcracks continues to grow, the glass produces microcracks, and the rupture area shows irregular expansion. In high temperatures, microcracks continue to sprout and develop, mainly exhibiting as along-crystal, intra-crystal, and through-crystal cracks exist in large numbers. The crack-linked network structure is formed, destroying the heat conduction between the particles. By approaching the number of loading steps to 25,301, the glass structure fails, the number of cracks no longer increases, and the microcrack area tends to be stabilized. During the loading stage, the number of cracks in the model is dominated by the longitudinal and small tangential cracks, indicating that the model is essentially controlled by tension cracking damage with a small amount of shear damage.

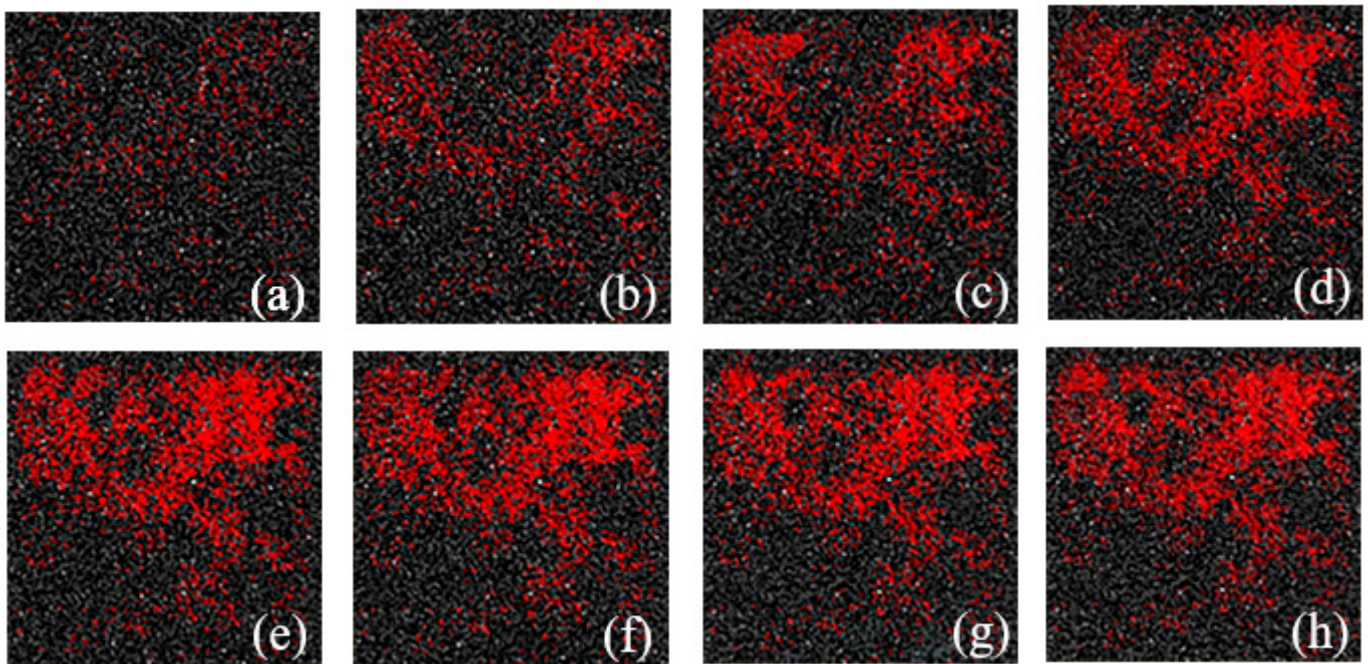


**Figure 7.** The microcrack characteristics of the float glass acted upon by the thermal loading, (a) The number of cracks at 5270 steps is 688, (b) The number of cracks at 9269 steps is 1612, (c) The number of cracks at 10,271 steps is 2279, (d) The number of cracks at 14,279 steps is 3670, (e) The number of cracks at 25,301 steps is 3682, (f) The number of cracks at 57,932 steps is 3682, (g) The number of cracks at 105,410 steps is 3682 and (h) The number of cracks at 188,210 steps is 3682.

Under thermal loading, glass behaves like a brittle material so that the microcracks can be readily developed as the stress and displacement fields change. Figure 8 demonstrates a cloud plot of the stress field distribution of the float glass under high-temperature loading. For the number of loading steps lower than 5270, the contact force distribution is relatively uniform, and no concentrated distribution occurs. Regarding the number of loading steps in the range of 5270–25,301, the glass is heated quickly since the temperature load in the normal direction generates large thermal stresses. In such a case, the constituting particles of the model move due to extrusion, and thereby, the contact forces between the particles increase, and the peak value of the contact force in the particle model increases by the growth of the thermal loading. When the number of loading steps exceeds 25,301, the contact force at the end of the crack gradually grows such that the concentration of the contact force produces microcracks. At the moment when the normal temperature load reaches its peak, the contact force at the end of the crack decreases, leading to the gradual reduction of the contact force inside the whole model. Subsequently, cracks are formed, and the squeezing effect between the constituent particles decreases, yielding the vanishing contact force in the middle section of the crack. Therefore, the peak contact force gradually lessens. At the later loading stage, the contact stress concentration zone on the inner boundary of the glass disappears, the contact force is completely released, and no new cracks are formed on the inner side of the glass. At this point, the crack expansion results from the continuous release of tensile stress.

### 3.4. Characteristics of the Microcrack Evolution

The number of microcracks in the glass increases with temperature growth, and their distribution is irregular. At 5270 steps of loading, large crack bands and large cracks are gradually produced between the glass particles. For the case of 7231 steps of loading, numerous small cracks join gradually and interconnect to form microcracks, accompanied by noticeably damaged areas. In the case of 25,301 steps of loading, the number of microcracks reaches a peak, and thereafter, the number and length of microcracks tend to be stabilized

at the temperature of about 650 °C. It is therefore believed that the microcracks in the float glass, under high-temperature action, first sprout continuously and then expand rapidly in the longitudinal and transverse directions, forming macrocracks.

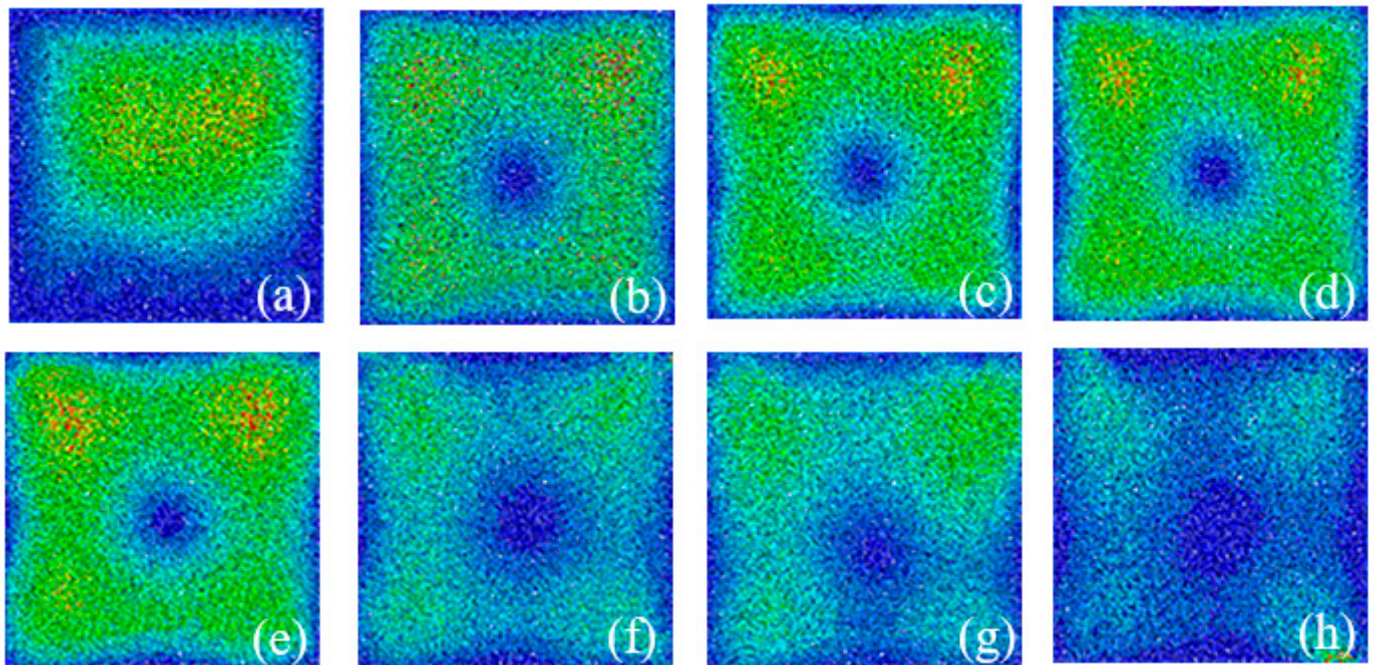


**Figure 8.** Characteristics of the stress field of the float glass under the action of high-temperature loading, (a) Peak stress of  $1.64 \times 10^5$  at 5270 steps, (b) Peak stress of  $1.64 \times 10^6$  at 9269 steps, (c) Peak stress of  $1.72 \times 10^6$  at 10,271 steps, (d) Peak stress of  $2.04 \times 10^6$  at 14,279 steps, (e) Peak stress of  $2.19 \times 10^6$  at 25,301 steps, (f) Peak stress of  $2.0 \times 10^6$  at 57,932 steps, (g) Peak stress of  $1.9 \times 10^5$  at 105,410 steps and (h) Peak stress of  $2.65 \times 10^4$  at 188,210 steps.

To reflect the temperature sensitivity of microcracks during loading,  $M_n$  is defined as the rate of change in the number of cracks in a given temperature range, calculated by:

$$M_n = \frac{N_{n+1} - N_n}{T_{n+1} - T_n} \quad (5)$$

where  $N_{n+1}$  and  $N_n$  to represent the number of microcracks in the glass at the  $(n + 1)$ -th and  $n$ -th stages of loading, while  $T_{n+1}$  and  $T_n$  denote their corresponding temperatures applied to the glass surface.

According to the numerical simulation results, the variation of  $M_n$  and the total number of microcracks with the loading temperature during the heating process has been plotted in Figure 9. During the loading process, the graph of  $M_n$  in terms of the loading temperature exhibits an oscillatory trend. This issue is because the generated thermal stress promotes the sprouting of the microcracks as well as their expansion in both longitudinal and transverse directions. At the beginning of loading, the  $M_n$  value fluctuates above and below of  $M_n = 3$ . When the temperature reaches 600 °C, the  $M_n$  suddenly increases and reaches a peak level; subsequently, the plots of  $M_n$  exhibit a large “oscillating” reduction as the temperature reaches 940 °C, the  $M_n$  value drops to 0 and remains unchanged. During the whole loading process, the trend of the total number of microcracks in terms of temperature increases sharply and then becomes stable.

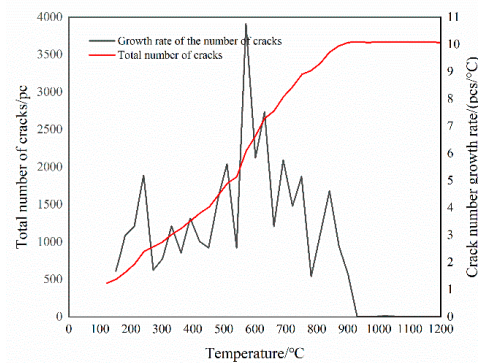


**Figure 9.** Characteristics of the microcracking as a function of the temperature.

Under thermal loading, microcracking occurs longitudinally and transversely in most cases. As demonstrated in Figure 10, with the increase in the number of thermal cycles, the cracks expand in the longitudinal direction in a “straight line”. During the formation and development of the glass microcracks, some of the microcracks gradually intersect and join each other to form a “tortoiseshell”.

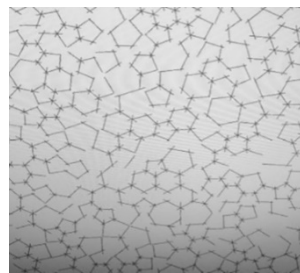


**Figure 10.** The microstructural characteristics of the microcracks in the float glass under high-temperature loading.

### 3.5. The Extension Mechanism of Microcracks

By analyzing the microstructure and process of microcrack origination and expansion within the glass in the presence of the thermal loading, it is found that the model failure process under thermal load can be divided into three apparent stages: microcrack emergence stage, microcrack expansion stage, and crack penetration failure stage.

In the microcrack emergence stage, crack emergence occurs throughout the micro rupture process, and crack initiation is discontinuous, following discontinuous emergence and expansion. The physical characteristics, such as the initial angle of the crack as well as the position of the crack nucleus, are mainly random and disordered. As the temperature grows, the damage zone gradually increases, mainly due to the differences in the connection bond and particle size as well as the thermal expansion characteristics of the particles, resulting in uncoordinated deformation. This issue yields a reduction in the ratio between the long and short axes of some of the microcracks during the warming process, forming a damage zone. At this stage, the cracks develop along the boundaries of the particles (see Figure 11a), where the emerging cracks originate and develop at the boundaries of the model particles or inside them. Then, the cracks are influenced by the shape, arrangement, and bond length of the glass particles during their formation, where the initial angles of the cracks exhibit their randomness.

In the microcrack extension stage, crack extension occurs within the model with a tendency to extend into the grain, and the direction of extension is perpendicular to the stress direction (see Figure 11b,e). After the model is uniformly heated during thermal loading, the difference in the internal thermal expansion coefficients leads to a non-uniform thermal expansion state for each structure, and various thermal strains will produce a non-uniform thermal stress field within the glass body. When the thermal stress is greater

than the yield limit of the material, microcrack extension occurs in both longitudinal and transverse directions.

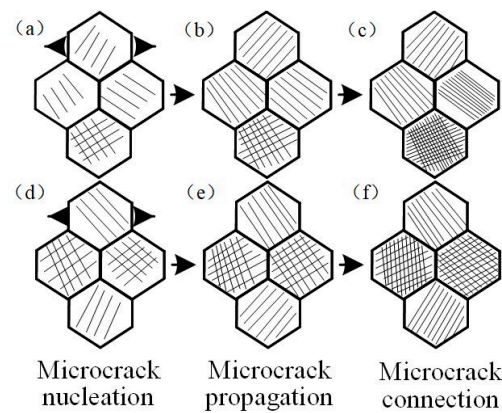


**Figure 11.** The microcrack initiation and expansion mechanism in the float glass under high-temperature action.

During the crack penetration failure stage (see Figure 11c,f), the glass particles are thermally expanded, and the number of small cracks grows as the load continues to increase. The grain boundary cracks of the model further expand along the grain boundary. In continuous thermal stress, the cracks along the grain and grain boundary cracks are connected, and numerous small cracks gradually join each other and interconnect to form macroscopic cracks.

The microscopic cracking mechanism of the heated glass can be further examined by the above microstructure cracking and extension. When the resulting thermal stress between the particles exceeds the corresponding tensile or shear bond strength, microcracks begin to sprout and expand along the boundaries of the constitutive particles. For the small thermal stresses, the large particles delay the expansion of the sprouting cracks, eventually forming dendritic cracks; however, when the thermal stress is large, these interlaced cracks form tortoise back cracks. Under the repeated action of thermal shock, the bonding of the particle interface fails, and the bonding damage and cracks at the grain interface become increasingly evident, eventually extending, joining, and penetrating each other to form macroscopic cracks, leading to the failure of the glass structure.

#### 4. Conclusions

(1) By conducting dimensional experiments, the rupture behavior of frame-supported float glass is elucidated from a macroscopic standpoint. Under thermal loading, the temperature difference between the sheltered and non-sheltered regions is identified as the main cause of the rupture of the frame-supported float glass. Based on the experimentally observed data, the critical temperature difference leading to glass rupture is reported to be about 65 °C. The time of the rupture is in 132–149 s, and the cracks commonly sprout from the edge of the glass surface with the greatest temperature difference. The cracks appear from the edge and then rapidly expand to the central region of the glass or other edges before stopping expansion. There are bifurcation cracks and shock cracks formed after the first rupture of the glass, and the cracks intersect to form crack islands, but no shedding phenomenon occurs.

(2) Based on the discrete element model for the thermally induced glass, the PFC<sup>2D</sup> program is adopted to establish a model for the microcracks generation in glass subjected to thermal fracturing. With the increase in the loading temperature, the number of microcracks in the glass sharply grows and then stabilizes, and the growth rate of the microcracks exhibits an oscillatory shape. The model is mainly broken and damaged by a small amount of shear damage. In the simulation of the 5270–25,301 step, the glass was formed in the 5270–10,271 step, which was in the glass center, which was located in the glass center,

and eventually reached the peak, the crack in the heat stress after 25,301, and the peak displacement increased (but the peak displacement concentration area was a gradual loss).

(3) The damage process of the glass acted upon by the thermal loading is commonly divided into three main stages: the crack initiation stage, the crack expansion stage, and the crack penetration failure stage. During the loading process, the microcrack emerges. When the heat stress between the particles exceeds the corresponding tensile or shear bond strength. When a specific temperature is reached, the expansion of microcracks becomes the main form. As the microcracks extend and connect, macroscopic cracks are formed, while the intersection of macroscopic cracks configures crack islands, eventually leading to the failure of the glass structure. In conjunction with experiments, the discrete element method can be exploited. The proposed numerical model can predict the temperature, stress distribution, and fracture behavior of glass, providing rational propositions for engineering applications.

**Author Contributions:** Conceptualization, J.D. and L.H.; methodology, Y.Z. and J.D.; software, Y.Z., L.H. and Z.F.; validation, Y.Z., L.H. and J.D.; formal analysis, D.Y.; investigation, X.L.; resources, S.Z.; data curation, D.Y. and X.L.; writing—original draft preparation, L.H. and Z.F.; writing—review and editing, Y.Z., J.D. and L.H.; visualization, X.L. and S.Z.; supervision, L.H.; project administration, Y.Z.; funding acquisition, Y.Z. All authors have read and agreed to the published version of the manuscript.

**Funding:** Shaanxi's Innovation Capability Support Program (Program No. 2020TD-021).

**Institutional Review Board Statement:** Not applicable.

**Informed Consent Statement:** Not applicable.

**Data Availability Statement:** The data presented in this study are available on request from the corresponding author. The data are not publicly available due to the particularity of the experimental data, the team may continue to study other data involved in the following work.

**Acknowledgments:** This work was supported by Shaanxi's Innovation Capability Support Program (Program No. 2020TD-021).

**Conflicts of Interest:** The authors declare no conflict of interest.

## References

1. Chow, W.K.; Hung, W.Y. Effect of cavity depth on smoke spreading of double-skin facade. *Build. Environ.* **2006**, *41*, 970–979. [[CrossRef](#)]
2. Wang, Y.; Sun, J.; He, L.; Wang, Q.; Rush, D. Experimental study on fallout behaviour of tempered glass facades with different frame insulation conditions in an enclosure fire. *Proc. Combust. Inst.* **2019**, *37*, 3889–3898. [[CrossRef](#)]
3. Sabsabi, A.; Youssef, M.A.; El-Fitiany, S.F.; Vedrtnam, A. Simplified structural analysis of framed ordinary non-tempered glass panels during fire exposure. *Fire Saf. J.* **2021**, *122*, 103357. [[CrossRef](#)]
4. Mauro, J.C.; Yue, Y.; Ellison, A.J.; Gupta, P.K.; Allan, D.C. Viscosity of glass-forming liquids. *Proc. Natl. Acad. Sci. USA* **2009**, *106*, 19780–19784. [[CrossRef](#)] [[PubMed](#)]
5. Cassetta, M.; Genova, D.G.; Zanatta, M.; Ballaran, T.B.; Kurnosov, A.; Giarola, M.; Mariotto, G. Estimating the viscosity of volcanic melts from the vibrational properties of their parental glasses. *Sci. Rep.* **2021**, *11*, 13072. [[CrossRef](#)]
6. Skelly, M.J.; Roby, R.J.; Beyler, C.L. An Experimental Investigation of Glass Breakage in Compartment Fires. *J. Fire Prot. Eng.* **1991**, *3*, 25–34. [[CrossRef](#)]
7. Emmons, H.W. The Needed Fire Science. *Fire Saf. Sci.* **1986**, *1*, 33–53. [[CrossRef](#)]
8. Pagni, P.J. Thermal glass breakage. *Fire Saf. Sci.* **2002**, *7*, 3–22. [[CrossRef](#)]
9. Joshi, A.A.; Pagni, P.J. *Users' Guide to BREAK1, The Berkeley Algorithm for Breaking Window Glass in a Compartment Fire*. National Institute of Standards and Technology Report No. NIST-GCR-91-596, Gaithersburg, Maryland. Available online: <https://books.google.com/books?id=vKdrrgEACAAJ> (accessed on 19 October 1999).
10. Harada, K.; Enomoto, A.; Uede, K.; Wakamatsu, T. An Experimental Study on Glass Cracking and Fallout by Radiant Heat Exposure. *Fire Saf. Sci.* **2000**, *6*, 1063–1074. [[CrossRef](#)]
11. Pope, N.D.; Bailey, C.G. Development of a Gaussian glass breakage model within a fire field model. *Fire Saf. J.* **2007**, *42*, 366–376. [[CrossRef](#)]
12. Hietaniemi, J. *Probabilistic Simulation of Glass Fracture and Fallout in Fire*; VTT Building and Transport: Vuorimiehentie, Finland, 2005.
13. Ni, Z.; Lu, S.; Peng, L. Experimental study on fire performance of double-skin glass facades. *J. Fire Sci.* **2012**, *30*, 457–472. [[CrossRef](#)]

14. Wang, Q.; Zhang, Y.; Sun, J.; Wen, J.; Dembele, S. Temperature and Thermal Stress Simulation of Window Glass Exposed to Fire. *Procedia Eng.* **2011**, *11*, 452–460. [[CrossRef](#)]
15. Wang, Q.; Zhang, Y.; Wang, Y.; Sun, J.; He, L. Dynamic three-dimensional stress prediction of window glass under thermal loading. *Int. J. Therm. Sci.* **2012**, *59*, 152–160. [[CrossRef](#)]
16. Wang, Q.; Chen, H.; Wang, Y.; Sun, J. Thermal Shock Effect on the Glass Thermal Stress Response and Crack Propagation. *Procedia Eng.* **2013**, *62*, 717–724. [[CrossRef](#)]
17. Wang, Q.; Wang, Y.; Chen, H.; Xiao, H.; Sun, J.; He, L. Frame constraint effect on the window glass crack behavior exposed to a fire. *Eng. Fract. Mech.* **2013**, *108*, 109–119. [[CrossRef](#)]
18. Wang, Q.; Chen, H.; Wang, Y.; Wen, J.; Dembele, S.; Sun, J.; He, L. Development of a dynamic model for crack propagation in glazing system under thermal loading. *Fire Saf. J.* **2014**, *63*, 113–124. [[CrossRef](#)]
19. Wong, D.; Li, K.; Spearpoint, M. A Probabilistic Model for the Fallout Area of Single Glazing under Radiant Heat Exposure. *Fire Saf. Sci.* **2014**, *11*, 444–457. [[CrossRef](#)]
20. Debuyser, M.; Sjostrom, J.; Lange, D.; Honfi, D.; Sonck, D.; Belis, J. Behaviour of monolithic and laminated glass exposed to radiant heating. *Constr. Build. Mater.* **2017**, *130*, 212–229. [[CrossRef](#)]
21. Wang, Y.; Wu, Y.; Wang, Q.; Liew, K.M.; Chen, H.; Sun, J.; He, L. Numerical study on fire response of glass facades in different installation forms. *Constr. Build. Mater.* **2014**, *61*, 172–180. [[CrossRef](#)]
22. Wang, Y.; Wang, Q.; Shao, G.; Chen, H.; Su, Y.; Sun, J.; He, L.; Liew, K.M. Fracture behavior of a four-point fixed glass curtain wall under fire conditions. *Fire Saf. J.* **2014**, *67*, 24–34. [[CrossRef](#)]
23. Wang, Y.; Wang, Q.; Su, Y.; Sun, J.; He, L.; Liew, K.M. Fracture behavior of framing coated glass curtain walls under fire conditions. *Fire Saf. J.* **2015**, *75*, 45–58. [[CrossRef](#)]
24. Wang, Y.; Wang, Q.; Wen, J.X.; Sun, J.; Liew, K.M. Investigation of thermal breakage and heat transfer in single, insulated and laminated glazing under fire conditions. *Appl. Therm. Eng.* **2017**, *125*, 662–672. [[CrossRef](#)]
25. Bedon, C. Structural Glass Systems under Fire: Overview of Design Issues, Experimental Research, and Developments. *Adv. Civ. Eng.* **2017**, *2017*, 2120570. [[CrossRef](#)]
26. Lu, W.; Duan, Q.; Chen, H.; Li, H.; Liu, Y.; Wang, Q.; Sun, J. Thermal response and resistance optimization of various types of point-supported glass facades. *Constr. Build. Mater.* **2019**, *224*, 610–621. [[CrossRef](#)]
27. Chen, H.; Wang, Y.; Zhang, Y.; Wang, Q.; Zhao, H.; Shao, G.; Su, Y.; Sun, J.; He, L. Crack evolution process of window glass under radiant heating. *Fire Mater.* **2017**, *41*, 1016–1026. [[CrossRef](#)]
28. Chen, H.; Wang, Q.; Wang, Y.; Zhao, H.; Sun, J.; He, L. Experimental and Numerical Study of Window Glass Breakage with Varying Shaded Widths under Thermal Loading. *Fire Technol.* **2017**, *53*, 43–64. [[CrossRef](#)]
29. Wang, Y.; Xie, Q.; Zhang, Y.; Wang, Q.; Sun, J. Sensitivity analysis of influencing factors on glass facade breakage in fire. *Fire Saf. J.* **2018**, *98*, 38–47. [[CrossRef](#)]
30. Wang, Y.; Zhang, Y.; Wang, Q.; Yang, Y.; Sun, J. The effect of glass panel dimension on the fire response of glass facades. *Constr. Build. Mater.* **2018**, *181*, 588–597. [[CrossRef](#)]
31. Al-Sibahy, A.; Edwards, R. Thermal behaviour of novel lightweight concrete at ambient and elevated temperatures: Experimental, modelling and parametric studies. *Constr. Build. Mater.* **2012**, *31*, 174–187. [[CrossRef](#)]
32. Shahpari, M.; Bamonte, P.; Mosallam, S.J. An experimental study on mechanical and thermal properties of structural lightweight concrete using carbon nanotubes (CNTs) and LECA aggregates after exposure to elevated temperature. *Constr. Build. Mater.* **2022**, *346*, 128376. [[CrossRef](#)]

**Disclaimer/Publisher’s Note:** The statements, opinions and data contained in all publications are solely those of the individual author(s) and contributor(s) and not of MDPI and/or the editor(s). MDPI and/or the editor(s) disclaim responsibility for any injury to people or property resulting from any ideas, methods, instructions or products referred to in the content.